Geophysical Research Letters

RESEARCH LETTER
10.1029/2022GL098485

Special Section:
ExoMars Trace Gas Orbiter - One Martian Year of Science

Variations in Vertical CO/CO$_2$ Profiles in the Martian Mesosphere and Lower Thermosphere Measured by the ExoMars TGO/NOMAD: Implications of Variations in Eddy Diffusion Coefficient

Nao Yoshida[1], Hiromu Nakagawa[1], Shohei Aoki[2], Justin Erwin[3], Ann Carine Vandaele[3], Frank Daerden[3], Ian Thomas[3], Loïc Trompet[3], Shungo Koyama[1], Naoki Terada[1], Lori Neary[3], Isao Murata[1], Geronimo Villanueva[4], Giuliano Liuzzi[4,5], Miguel Angel Lopez-Valverde[6], Adrian Brines[6], Ashimananda Modak[6], Yasumasa Kasaba[1], Bojan Ristic[3], Giancarlo Bellucci[7], José Juan López-Moreno[6], and Manish Patel[8]

[1]Graduate School of Science, Tohoku University, Sendai, Japan, [2]Graduate School of Frontier Sciences, University of Tokyo, Kashiwa, Japan, [3]Royal Belgian Institute for Space Aeronomy, BIRA-IASB, Brussels, Belgium, [4]NASA Goddard Space Flight Center, Greenbelt, MD, USA, [5]Department of Physics, American University, Washington, DC, USA, [6]Instituto de Astrofisica de Andalucia (IAA/CSIC), Granada, Spain, [7]Institute di Astrofisica e Planetologia Spaziali (IAPS/INAF), Rome, Italy, [8]School of Physical Sciences, The Open University, Kents Hill, UK

Key Points:

- The CO/CO$_2$ profiles from 75 to 105 km measured by NOMAD aboard TGO are used to investigate variations in the eddy diffusion coefficient
- The estimated CO/CO$_2$ profiles agree well with the observed profiles if altitude-dependent eddy diffusion coefficients are considered
- Our results demonstrate a substantial seasonal variation in the eddy diffusion coefficient in the southern hemisphere

Supporting Information:

Supporting Information may be found in the online version of this article.

Correspondence to:

N. Yoshida,
nao.yoshida.q7@dc.tohoku.ac.jp

Citation:

Yoshida, N., Nakagawa, H., Aoki, S., Erwin, J., Vandaele, A. C., Daerden, F., et al. (2022). Variations in vertical CO/CO$_2$ profiles in the Martian mesosphere and lower thermosphere measured by the ExoMars TGO/NOMAD: Implications of variations in eddy diffusion coefficient. *Geophysical Research Letters*, *49*, e2022GL098485. https://doi.org/10.1029/2022GL098485

Received 28 FEB 2022
Accepted 7 MAY 2022

Author Contributions:

Conceptualization: Nao Yoshida, Naoki Terada
Data curation: Ian Thomas
Funding acquisition: Nao Yoshida, Ann Carine Vandaele
Investigation: Nao Yoshida

Abstract Using the Nadir and Occultation for MArs Discovery instrument aboard Trace Gas Orbiter, we derived the CO/CO$_2$ profiles between 75 and 105 km altitude with the equivalent width technique. The derived CO/CO$_2$ profiles showed significant seasonal variations in the southern hemisphere with decreases near perihelion and increases near aphelion. The estimation of the CO/CO$_2$ profiles with a one-dimensional photochemical model shows that an altitude-dependent eddy diffusion coefficient better reproduces the observed profiles than a vertically uniform one. Our estimation suggests that the eddy diffusion coefficient in L_s = 240–270 is uniformly larger by a factor of ∼2 than that in L_s = 90–120 in the southern hemisphere, while they are comparable in the northern hemisphere. This fact demonstrates that the eddy diffusion coefficient is variable with season and latitude.

Plain Language Summary The eddy diffusion coefficient is widely used to parameterize the efficiency of vertical diffusion in the planetary atmosphere, whose variation characterizes the transportation of trace gas species. Additionally, it could vary their vertical distributions in the middle and upper atmosphere, which might cause an impact on the species escaping to space. However, the variability of the eddy diffusion coefficient in those altitude regions have been poorly understood. In this study, we focus on the estimation of variation in the eddy diffusion coefficient by analyzing the CO and CO$_2$ measurements made by the ExoMars Trace Gas Orbiter. The observed CO/CO$_2$ ratio between altitudes of 75 and 105 km shows a significant seasonal variation in the southern hemisphere. The observed CO/CO$_2$ profiles are compared with the simulated profiles obtained with a one-dimensional photochemical model assigning several shapes and intensity of eddy diffusion coefficient. The comparison shows that the eddy diffusion coefficient is not constant but variable depending on altitude, season, and latitude, which suggests that the efficiency of the vertical diffusion varies with season and latitude. This fact is useful to other 1D photochemical models to reproduce the seasonal and latitudinal variation of atmospheric composition.

1. Introduction

CO is produced by the photodissociation of CO$_2$ and recycled to CO$_2$ by the catalytic cycle involving HOx in the Martian atmosphere (e.g., McElroy & Donahue, 1972). The photochemical lifetime of CO is ∼6 years in the lower atmosphere (Krasnopolsky, 2007). The previous nadir observations revealed latitudinal and seasonal distributions of CO in the lower atmosphere, which indicate CO$_2$ condensation/sublimation in the polar caps and dynamics (Encrenaz et al., 2006; Smith et al., 2009, 2021). In the middle and upper atmosphere (>∼50 km), the photochemical lifetime of CO becomes much longer due to the decrease in HOx species density. Thus, the characteristic times of production and eddy diffusion of CO are shorter than the photochemical lifetime of CO in

Methodology: Nao Yoshida, Shohei Aoki, Justin Erwin
Project Administration: Ann Carine Vandaele, Bojan Ristic, Giancarlo Bellucci, José Juan López-Moreno, Manish Patel
Resources: Ann Carine Vandaele, Frank Daerden, Ian Thomas, Loïc Trompet, Shungo Koyama, Lori Neary, Giuliano Liuzzi, Miguel Angel Lopez-Valverde, Adrian Brines, Bojan Ristic
Supervision: Hiromu Nakagawa, Ann Carine Vandaele, Naoki Terada, Yasumasa Kasaba
Validation: Nao Yoshida, Shohei Aoki, Loïc Trompet, Isao Murata, Miguel Angel Lopez-Valverde, Ashimananda Modak
Visualization: Nao Yoshida
Writing – original draft: Nao Yoshida
Writing – review & editing: Hiromu Nakagawa, Shohei Aoki, Justin Erwin, Ann Carine Vandaele, Frank Daerden, Ian Thomas, Shungo Koyama, Miguel Angel Lopez-Valverde, Manish Patel

the mesosphere and lower thermosphere. When we interpret seasonal variations of CO in the middle and upper atmosphere, contributions from the eddy diffusion and from production need to be considered.

The eddy diffusion coefficient is used to parameterize the efficiency of the vertical diffusion, which has been estimated from vertical profile of atmospheric composition (e.g., Rodrigo et al., 1990). However, there is a considerable uncertainty between altitudes of 40 and 90 km, and then an empirical profile has typically been used in the 1D models. For example, based on the observation of atmospheric composition and the estimation of eddy diffusion coefficient near the aphelion, Krasnopolsky (2006) simply assumed two times larger eddy diffusion coefficient near the perihelion compared to the aphelion. Recently, a substantial variation in the eddy diffusion coefficient at the homopause altitude has been suggested (Slipski et al., 2018) as well as a large fluctuation of the homopause altitude (Jakosky et al., 2017; Slipski et al., 2018; Yoshida et al., 2020). These recent studies imply a strong variability of the eddy diffusion coefficient around the altitude of the homopause (60–140 km). A substantial variation of the homopause altitude changes the boundary altitude above which gases are diffusively separated according to their mass by molecular diffusion. Therefore, the location of the homopause altitude and eddy diffusion coefficient in that region are important for the thermospheric composition (Yoshida et al., 2020, 2021) and the subsequent escape of species to space. Meanwhile, the homopause altitude and the eddy diffusion coefficient at that altitude have been estimated using the atmospheric composition in the thermosphere observed by the Mars Atmosphere and Volatile Evolution (MAVEN) spacecraft, which cannot observe the mesosphere regularly.

According to general circulation models (GCM), the CO mixing ratio in the mesosphere and thermosphere increases with altitude due to the photodissociation of CO_2, and it is enhanced in the polar region due to the meridional circulation (Daerden et al., 2019; Holmes et al., 2019). Recently, Trace Gas Orbiter (TGO) observed the vertical distribution of CO for the first time in the mesosphere and lower thermosphere. Olsen et al. (2021) confirmed that their observations using the Atmospheric Chemistry Suite (ACS) (Korablev et al., 2018) aboard TGO showed similar trends as GCM simulations. They also found a decrease in CO mixing ratio after the onset of the global dust storm in MY 34 and an enhancement in the CO mixing ratio in polar regions. However, CO distribution has not been studied with respect to variations in the eddy diffusion coefficient. The solar occultation channel (SO) of the Nadir and Occultation for MArs Discovery (NOMAD) instrument aboard TGO, provides regular measurements of CO and the opportunity to directly discuss the variation of eddy diffusion coefficients. A companion paper in this special issue by Modak et al. (2022) describes the CO distribution in MY 34 using NOMAD SO observations.

The purposes of this study are (a) to retrieve the CO/CO_2 profiles derived from NOMAD measurements, (b) to investigate the variability in the CO/CO_2 profiles in the Martian mesosphere and lower thermosphere, and (c) to clarify the variation of the eddy diffusion coefficient using a 1D photochemical model. The CO distribution during the global dust storm in MY 34 is presented in Olsen et al. (2021). In this study, we focus on the seasonal variation of CO and excluded the data set in MY 34 to avoid the effect of the global dust storm. We introduce the NOMAD instrument, data set, and retrieval method in Section 2. The results and discussion of the 1D photochemical model will be described in Sections 3 and 4, respectively. Our conclusions are summarized in Section 5.

2. Method

2.1. Instrument and Observations

NOMAD aboard TGO was designed to explore the composition and distribution of Mars' atmospheric trace gas species (Vandaele et al., 2015). The SO channel of NOMAD probes the Martian atmosphere in the IR region delivering vertical profiles of trace gases (e.g., Aoki et al., 2019; Vandaele et al., 2019). NOMAD SO measures transmittance spectra in the wavelength range of 2.2–4.3 μm (2,320–4,350 cm^{-1}) with relatively high spectral resolution ($R = 17{,}000$) thanks to the combination of an Acousto Optical Tunable Filter (AOTF) and an echelle grating (Neefs et al., 2015; Thomas et al., 2016; Vandaele et al., 2018). The AOTF instantaneously selects the diffraction order that will be recorded; five or six different orders are sequentially probed within a second during an occultation, leading to a vertical sampling of the spectra less than 1 km. NOMAD SO measures spectra from the Mars near-surface to 250 km altitude, and CO and CO_2 absorption features appear below about 100 and 180 km altitudes, respectively.

Recently, the calibration of the SO channel has been extensively updated (Villanueva et al., 2022). In this update, the AOTF transfer function has been reevaluated using inflight solar measurements, which allows us to

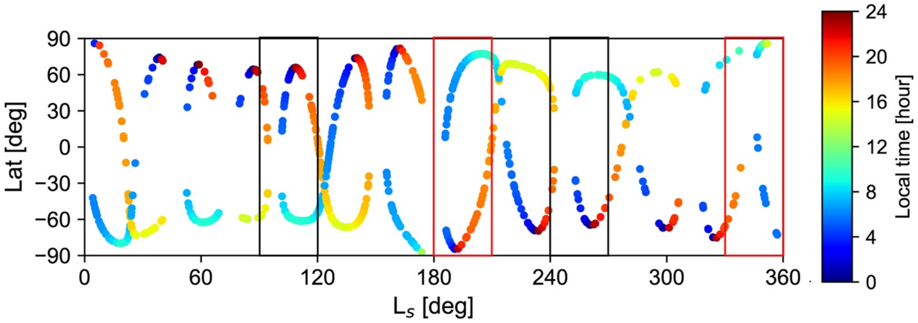

Figure 1. Coverages of the NOMAD SO orbits during MY 35, which are analyzed in this study. The data set is limited to orbits when orders 190 and 149 are measured simultaneously. The color represents the local time. The red and black rectangles indicate the subdata sets shown in Figures 3 and 4, respectively.

significantly reduce the uncertainty and perform the molecular retrievals properly (Villanueva et al., 2022). The characterization of the instrumental line shape (ILS) has also been updated. It was found that the ILS is not a simple Gaussian function but has an asymmetric shape (Thomas et al., 2021) that can be reproduced by a combination of two Gaussian functions (Villanueva et al., 2022). These latest updated instrumental functions were used in this analysis.

TGO/NOMAD has been operating from April 2018 up to now. This study focusses on the profiles observed in MY 35 corresponding to the 25 March 2019 to 6 February 2021 period. Since TGO has a polar orbit, the NOMAD SO channel can observe at most 24 times per 1 sol. However, diffraction orders that contain CO and CO_2 lines are not always observed together. In this study, we used only the orbits which measured CO spectra features in order 190 (4269.95–4303.99 cm^{-1}) and CO_2 spectra features in order 149 (3348.54–3375.23 cm^{-1}), simultaneously, as such the total number of orbits is limited to 649. The geometry of these selected orbits is shown in Figure 1, which demonstrates that the data set covers the whole period of MY 35, whereas sampling latitude and local times gradually vary with solar longitudes.

2.2. Retrieval

In this study, we applied the equivalent width technique (Chamberlain & Hunten, 1987; Krasnopolsky, 1986) to derive CO and CO_2 total column densities along the line of sight (hereafter, called "slant column") from the NOMAD spectra. The advantage of this method is that it is computationally very fast. The disadvantages of this method are (a) it can only be applied to a limited altitude range; and (b) we have to assume a homogeneous atmosphere along the line of sight. According to the curve of growth theory, the area of absorption line is proportional to slant column density as long as the absorption line is not saturated. This can be used to derive the slant column density given by $W = SN$, where W is the area of absorption, N is the slant column density of the molecule along the line of sight, and S is the line strength. The target lines should be isolated from other lines to apply the equivalent width technique. We carefully selected the CO lines centered at 4288.2 and 4291.5 cm^{-1} in order 190 and CO_2 lines at 3355.7, 3357.2, 3358.7, and 3360.3 cm^{-1} in order 149. The isolation of lines from the adjacent lines is illustrated in Supporting Information S1. To derive the area of absorption feature, we fitted the measured spectra within ± 1 cm^{-1} from the line center with a function of the ILS for each line. The area is converted to slant column density considering the transmission efficiency of the AOTF and the diffraction efficiency of the Blaze function. Since the line intensities of CO and CO_2 vary depending on temperature, we used the temperature at the tangential point predicted by the GEM-Mars model (Daerden et al., 2019) for retrieval. Examples of fitting and derived slant column densities are shown in Figure 2. The residuals after the fitting are within the level of instrumental noise. The calculated CO and CO_2 slant column densities are restricted to where those slant opacities are less than one. The selected lines are saturated where slant column densities reach $\sim 10^{18}$ cm^{-2} for CO and $\sim 10^{21}$ cm^{-2} for CO_2, respectively. We also set the upper limit of the valid altitude where SNR of absorption depth equals four to exclude the noisy measurements. The available altitudes vary with seasons and locations (Figures 2h and 2i). The derived slant column density has an uncertainty of 5–14% for CO (5–20% for CO_2). The retrieved CO and CO_2 slant column densities at each absorption line agree within the uncertainties. Finally, the CO/CO_2 profiles are binned in altitude over an interval of 1 km. The uncertainty of CO/CO_2 is 6–24%.

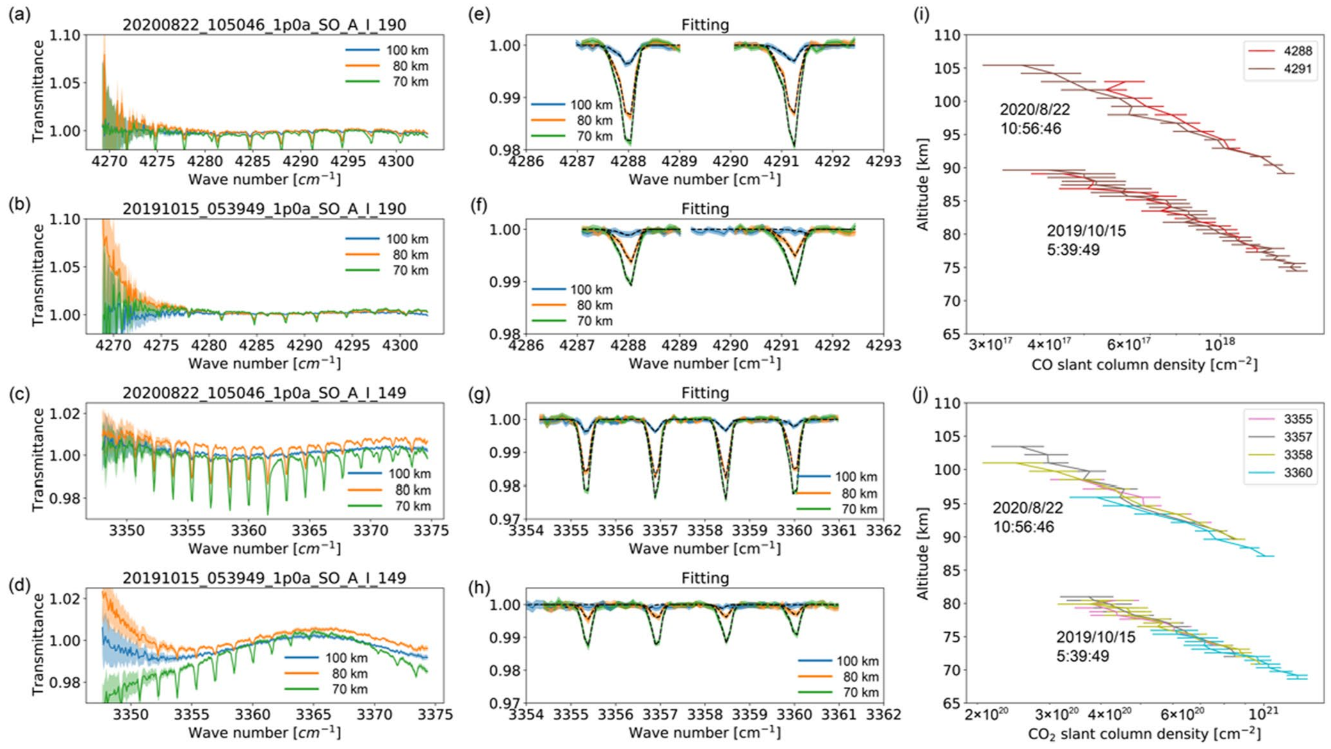
(a) 20200822_105046_1p0a_SO_A_I_190

(b) 20191015_053949_1p0a_SO_A_I_190

(c) 20200822_105046_1p0a_SO_A_I_149

(d) 20191015_053949_1p0a_SO_A_I_149

(e) Fitting

(f) Fitting

(g) Fitting

(h) Fitting

Figure 2. Examples of fitting and derived slant column densities. The top five panels (a, b, e, f, and i) are for order 190 (CO), and the bottom five panels (c, d, g, h, and j) are for order 149 (CO_2). As examples of profiles in the southern winter and summer seasons, we show two transmittances and retrieved results: corresponding to measurements obtained on 22 August 2020 at 10:50:46, at 64°S, 22 hr, 263°L_s; and on 15 October 2019 at 5:39:49, at 50°S, 15 hr, 93°L_s. (a, b, c, and d) Transmittances at 70, 80, and 100 km altitudes, respectively. (e, f, g, and h) Normalized transmittance at the same altitudes and best fit (black dashed line) are shown around the absorption features used for the retrieval. The uncertainty of the transmittance is shown as the shadow. The fit was applied on a spectral interval centered on the line within ±1 cm^{-1}. (i, j) Derived slant column densities at altitudes where the absorption lines are not saturated.

We assume that the CO/CO_2 profile, derived from the slant column densities of CO and CO_2, is coming from the information at the tangent altitude height. The accuracy of the slant column density derived from the equivalent width technique has been evaluated by comparison with that derived from the retrievals using the full radiative transfer calculation with ASIMUT (Vandaele et al., 2006). The CO and CO_2 retrievals by ASIMUT were performed based on the Optimal Estimation Method (OEM) (Rodgers, 2000). We found that the both CO and CO_2 slant column densities derived by the equivalent width technique are systematically deviated from that by ASIMUT. This discrepancy is due to the fact that the equivalent width is assumed as linear up to an optical depth of 1. However, those systematic discrepancies are canceled out to some extent while deriving the CO/CO_2 profiles. The CO/CO_2 ratio derived from our method is systematically small by ∼10–20% in L_s = 90–120, 180–210, and 330–360, meanwhile, there is a less statistical difference between our method and the ASIMUT in L_s = 240–270. The detailed comparison with the ASIMUT is described in the supporting material. We pay no attention to this discrepancy since it is comparable to the uncertainty, however, it is better to use a full radiative transfer code to derive the correct number densities. Additional uncertainty arises from the accuracy of GEM-Mars temperature, which is estimated to be within ±10 K compared with the retrieved temperature (Trompet et al., 2021). When we shift the temperature to ±10 K according to the uncertainty, the derived slant column density changes each line and altitude; the CO/CO_2 profiles have uncertainty within 15%. However, it is difficult to determine the exact value of the uncertainty of the GEM-Mars model. We only deal with the uncertainty derived from the best fit to the absorption line.

3. Results

Figure 3 shows the retrieved vertical profiles of CO/CO_2 in L_s = 90–120, 180–210, 240–270, and 330–360 in MY 35. The northern and southern hemispheres are separated. To distinguish the enhancement in polar regions (>70°) due to the meridional circulation from the thermosphere, latitude is separated. The CO/CO_2 ratio is

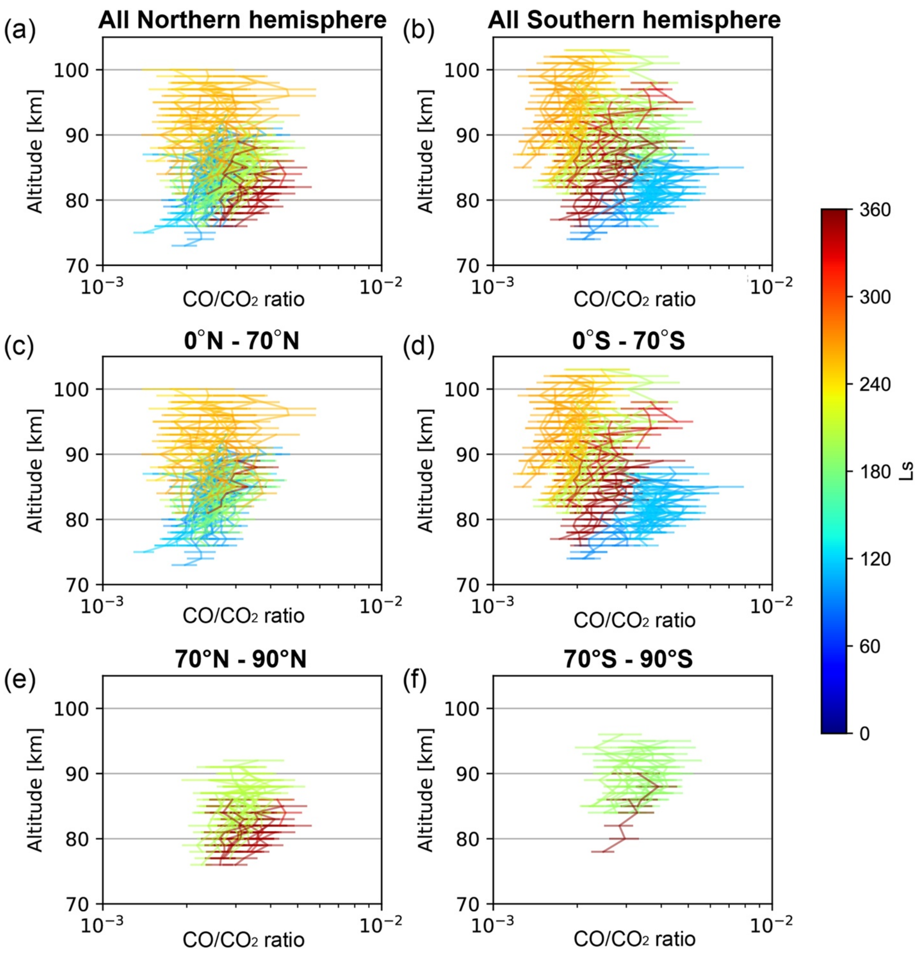

Figure 3. Vertical profiles of the CO/CO$_2$ ratio in L_s = 90–120, 180–210, 240–270, and 330–360. Horizontal lines are error bars. Color represents L_s. Profiles are separated into the northern (a, c, and e) and southern (b, d, and f) hemispheres. To distinguish the enhancement in polar regions, profiles are separated into two latitudinal bins: from the equator to 70° (c) and (d) and 70–90° (e, f).

typically retrieved between 75 and ~105 km. Overall, it increases with altitude, however, the mixing ratio of some profiles remains constant as shown in the supporting material. That is consistent with the results by ACS aboard TGO (Olsen et al., 2021). The observed CO/CO$_2$ ratios at 85 km range from ~1,500 to ~5,000 ppm, which is also consistent with the CO/CO$_2$ ratio reported in Olsen et al. (2021).

We found that the variability of the CO/CO$_2$ ratio is different in the two hemispheres. A significant seasonal variation in the CO/CO$_2$ ratio is found in the southern hemisphere, where it decreases near the perihelion and increases near the aphelion. Meanwhile, less discernible variation in the CO/CO$_2$ profiles appears in the same L_s ranges in the northern hemisphere. It is noted that the CO/CO$_2$ ratio is systematically small by 10–20% except for L_s = 240–270 as described above, however, those systematic bias is small compared to the seasonal variation in the southern hemisphere and comparable to the variability of each data set in the northern hemisphere. We can also see the latitudinal variation in the solstice season. The CO/CO$_2$ ratio becomes larger (smaller) in the southern hemisphere than in the northern hemisphere in the southern winter season (southern summer season). This is likely due to the fact that the CO$_2$ sublimation from the polar cap is stronger in the southern hemisphere than in the northern hemisphere (Daerden et al., 2019). However, our observation cannot directly discuss this issue because of the limited altitude range.

In the L_s = 180–210 and 330–360, the NOMAD SO observations cover all latitudes from the equator to the polar region. The enhancement of the CO/CO$_2$ ratio in polar regions is measured at both hemispheres (Figures 3e and 3f), which agrees with the result by ACS (Olsen et al., 2021) and has also been predicted by the GEM-Mars simulations (Daerden et al., 2019). It is attributed to the meridional circulation in the upper atmosphere.

In the next section, we discuss the seasonal variation in the observed CO/CO_2 profiles using a 1D photochemical model.

4. Discussion

A 1D time-dependent photochemical model (Koyama et al., 2021, modified after; Chaffin et al., 2017) has been used to interpret the observed seasonal variations of the CO/CO_2 ratio. Here, we only summarize the key points of the model. More details can be found in Chaffin et al. (2017). The model solves the continuity flux equations and photochemistry at each altitude. It includes 13 C-bearing, H-bearing, and O-bearing species and 54 photochemical reactions following Chaffin et al. (2017). However, we removed HOCO since the initial atmosphere used as input does not include HOCO (the initial atmosphere is described later). The upper boundary condition for O is the fixed escape rate of 1.2×10^8 cm^{-2} s^{-1}. Those for H and H_2 are assumed to be Jeans thermal escape rates. The deposition fluxes of all species are not included in this study. Molecular and thermal diffusion coefficients are applied from Banks and Kockarts (1973) and Krasnopolsky (2002), respectively. The initial atmospheric profile is chosen as the annually averaged profile of the GEM-Mars model (Daerden et al., 2019) because 1D photochemical models have inherent difficulties about the CO mixing ratio at the surface (cf. Krasnopolsky, 2010 and references therein). The inclusion of temperature profiles simulated by GEM allows for a more accurate estimation of the dynamics and photochemistry in the 1D photochemical model. The temperature profiles inputted in the model are described in Supporting Information S1. The variations in heliocentric distances are taken into account in the model input.

To investigate the contribution of the variability of the eddy diffusion coefficient in each hemisphere, we calculated the CO/CO_2 ratios considering two cases: (a) the eddy diffusion coefficients are vertically uniform; (b) the vertical profile of eddy diffusion coefficients is given by $K(z) = An(z)^{-1/2}$, where A is a constant, and $n(z)$ is the total number density at certain altitude. We first set the eddy diffusion coefficients being constant with altitude, with magnitudes ranging from 10^5 to 10^8 cm^2 s^{-1} for every one-half order of magnitude according to the estimation that the eddy diffusion coefficient equals the molecular diffusion coefficient at the homopause altitude (Slipski et al., 2018). Second, we assumed the eddy diffusion coefficients as $K(z) = An(z)^{-1/2}$ assigning different numerical values from 4×10^{13} to 2×10^{14} in steps of 0.25 to A. The altitude-dependent estimation of the eddy diffusion coefficient follows the approximation of internal wave activity and conservation of energy density (Lindzen, 1971). In both cases, after we change the eddy diffusion coefficient and temperature profile at time = 0, the CO/CO_2 profiles first respond to diffusion and production due to the photodissociation of CO_2 and then respond to photochemical loss with the OH density in the lower atmosphere. The response to photochemical loss between 75 and 105 km altitude is too slow (more than 10^{11} s) compared with the time scale of the diffusion ($\sim 10^6$ s at 75 km for $K = 10^6$ cm^2 s^{-1}) and production (10^6 s at 75 km). Thus, we hereafter show the profiles after 10^7 s when the CO/CO_2 profiles reach steady states due to diffusion and production. The CO_2 densities and temperature are linked through the hydrostatic equilibrium, while the CO number densities respond to both temperature and the eddy diffusion coefficient. Thus, the CO/CO_2 ratio varies with the eddy diffusion coefficient and temperature. We evaluated the response of the CO/CO_2 ratio to temperature (described in Supporting Information S1), which suggests that variations in the eddy diffusion coefficient need to be taken into account to reproduce the seasonal variations in the CO/CO_2 profiles as observed in this study. The best eddy diffusion coefficient is determined using a chi-square test between the observed CO/CO_2 ratio and the estimated CO/CO_2 ratio.

In the case of the vertically uniform eddy diffusion coefficient, the eddy diffusion coefficients of $K = 5 \times 10^6$ cm^2 s^{-1} for $L_s = 90$–120 in the northern and southern hemispheres are determined to reproduce the observed CO/CO_2 ratio (Figures 4a and 4c). For $L_s = 240$–270, the larger eddy diffusion coefficients of $K = 10^7$ cm^2 s^{-1} in the northern and southern hemispheres are estimated (Figures 4a and 4c). The estimated CO/CO_2 profiles with the vertically uniform eddy diffusion coefficient do not agree with the observed one except for $L_s = 90$–120 in the southern hemisphere.

When we assume an altitude-dependent eddy diffusion profile, following the expression $K(z) = An(z)^{-1/2}$, the observed CO/CO_2 profiles are reproduced more correctly. In the northern hemisphere, we found that $K(z) = 1.25 \times 10^{14} n(z)^{-1/2}$ cm^2 s^{-1} for $L_s = 240$–270 and $K(z) = 7 \times 10^{13} n(z)^{-1/2}$ cm^2 s^{-1} for $L_s = 90$–120 provide the best fit

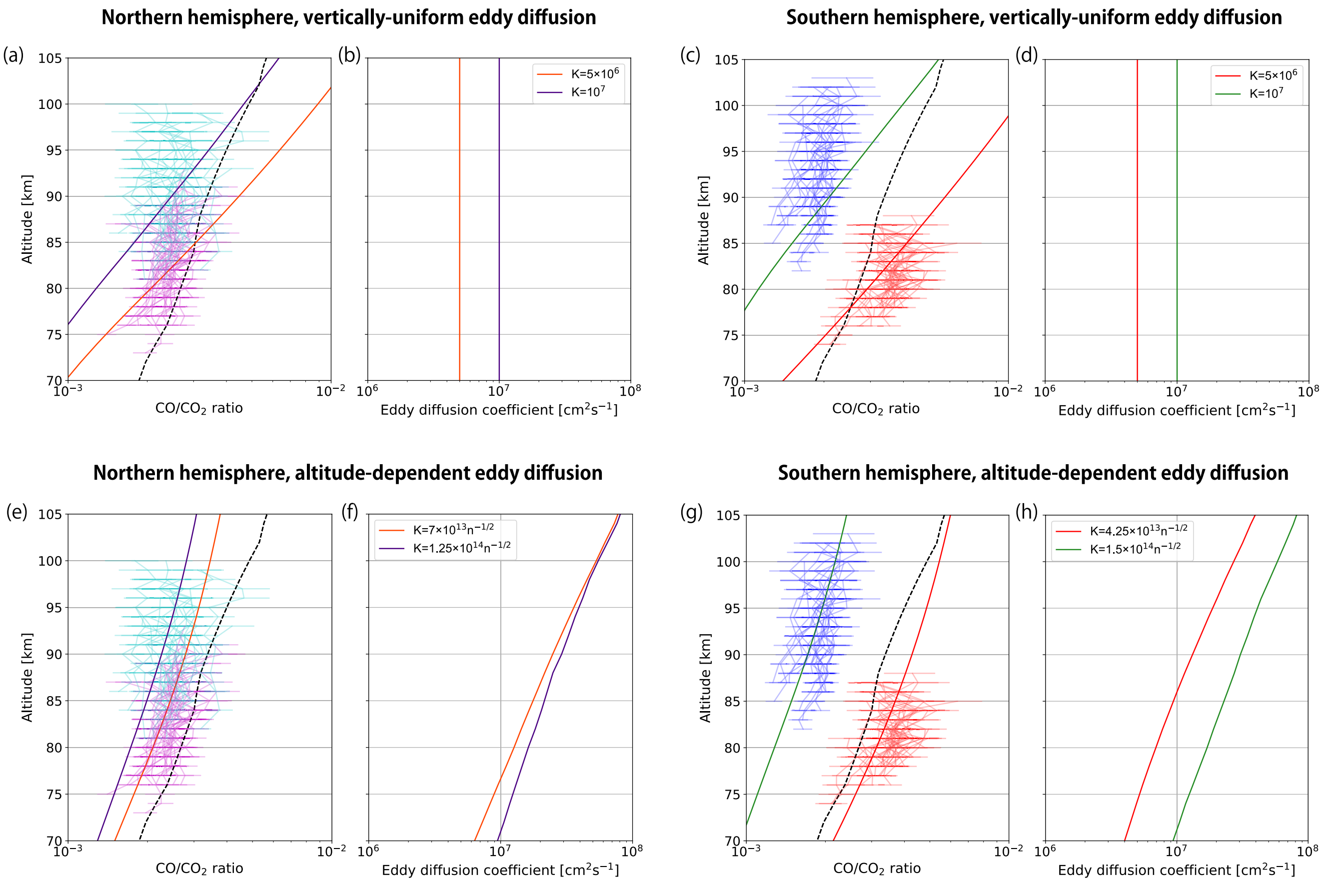

Figure 4. (a, c, e, and g) Vertical profiles of the CO/CO$_2$ ratio estimated with the 1D model and observed by NOMAD SO. The broken lines represent the initial CO/CO$_2$ profiles in the model. For the northern (southern) hemisphere, the observed CO/CO$_2$ profiles in L_s = 240–270 are shown in light blue (blue), and those in L_s = 90–120 are in magenta (red). (b, d, f, and h) The determined eddy diffusion coefficients by the 1D model. Profiles are distinguished by colors and divided into two hemispheres.

(Figures 4e and 4f). Estimated eddy diffusion coefficients are 1.4 times larger in L_s = 240–270 at 75 km altitude, however, its differences are gradually discernible above 75 km. In the southern hemisphere, the best fit eddy diffusion coefficients are $K(z) = 1.5\times10^{14}n(z)^{-1/2}$ cm^2 s^{-1} for L_s = 240–270 and $K(z) = 4.25\times10^{13}n(z)^{-1/2}$ cm^2 s^{-1} for L_s = 90–120 (Figures 4g and 4h). The estimated eddy diffusion coefficient in L_s = 240–270 is almost two times larger throughout the altitude range than that in L_s = 90–120. It is suggested that the larger variations in the eddy diffusion coefficient are necessary to reproduce the CO/CO$_2$ seasonal variations in the southern hemisphere compared to that in the northern hemisphere. A systematical bias of CO/CO$_2$ ratio in L_s = 90–120 corresponds to ~10% (~20%) differences for eddy diffusion coefficients in the southern (northern) hemisphere during the same L_s range. That is smaller than the estimated seasonal variation in the eddy diffusion coefficient and does not affect our conclusion. To our knowledge, this is the first time that the seasonal and latitudinal variations in the eddy diffusion coefficient have been suggested. The difference between the season and latitude might suggest a difference in the vertical diffusion efficiency. In our estimation, the mixing due to both the circulation and wave-induced eddy is blended. To discuss them, we need to estimate the intensity of the vertical diffusion due to the circulation and internal waves, respectively, however, this is the out of scope of this paper.

For application to another 1D model, a typical eddy diffusion coefficient near aphelion and perihelion would be helpful. When we put together the variation in both the northern and southern hemispheres, eddy diffusion coefficient in L_s = 90–120 is $K(z) = 6.75\times10^{13}n(z)^{-1/2}$ and that in L_s = 240–270 is $K(z) = 1.5 \times 10^{14}n(z)^{-1/2}$, which means ~1.3 times larger eddy diffusion coefficient in L_s = 240–270.

5. Summary

We investigated the CO/CO_2 ratio variations between 75 and 105 km using CO and CO_2 slant column densities derived from the SO channel of NOMAD abroad TGO using the equivalent width technique. The observed CO/CO_2 profiles show seasonal and latitudinal variations. We estimated the eddy diffusion coefficient with a 1D photochemical model using the observed CO/CO_2 profiles. It is suggested that the eddy diffusion coefficient expressed by $K(z) = An(z)^{-1/2}$ is a better assumption than the vertically uniform eddy diffusion coefficient. The simulations also suggest seasonal and latitudinal variability of the eddy diffusion coefficients in the Martian atmosphere. Two times larger eddy diffusion coefficient is proposed in the southern summer season, which might suggest that vertical diffusion is more efficient in the southern hemisphere near perihelion.

The detailed examination of the eddy diffusion coefficient between the mesosphere to the thermosphere (cf. Mahieux et al., 2021) will be conducted with CO and CO_2 number densities and temperature profiles retrieved from SO channel of NOMAD using ASIMUT. An accurate eddy diffusion coefficient will be much more useful for the parameterization of a 1D photochemical model and GCM model. In addition, the CO distribution retrieved from NOMAD SO from the near-surface to ∼100 km will contribute to understanding the dynamics and photochemistry of CO on Mars comparing GCM model. Local time variation has not been distinguished due to the combination of geometry among local time, latitude, and L_s in this study, however, it will be investigated in the future with more additional data set.

Data Availability Statement

The results retrieved from NOMAD SO with equivalent width technique used in this study are available at https://dx.doi.org/10.18758/71021076.

Acknowledgments

The NOMAD experiment is led by the Royal Belgian Institute for Space Aeronomy (IASB-BIRA), assisted by Co-PI teams from Spain (IAA-CSIC), Italy (INAF-IAPS), and the United Kingdom (Open University). This project acknowledges funding by the Belgian Science Policy Office (BELSPO), with the financial and contractual coordination by the ESA Prodex Office (PEA 4000103401, 4000121493), by Spanish Ministry of Science and Innovation (MCIU) and by European funds under Grants PGC2018-101836-B-I00 and ESP2017-87143-R (MINECO/FEDER), as well as by UK Space Agency through Grants ST/V002295/1, ST/V005332/1, and ST/S00145x/1 and Italian Space Agency through Grant 2018-2-HH.0. This work was supported by the Belgian Fonds de la Recherche Scientifique–FNRS under Grant No. 30442502 (ET_HOME). The IAA/CSIC team acknowledges financial support from the State Agency for Research of the Spanish MCIU through the "Center of Excellence Severo Ochoa" award for the Instituto de Astrofísica de Andalucía (SEV-2017-0709). US investigators were supported by the National Aeronautics and Space Administration. Canadian investigators were supported by the Canadian Space Agency. Y. N. is supported by The international Joint Graduate Program in Earth and Environmental Sciences, Tohoku University (GP-EES), and the Japanese Society for the Promotion of Science (JP21J13710). This work was supported by JSPS KAKENHI Grant Nos. 20H04605 and 19K03943.

References

Aoki, S., Vandaele, A. C., Daerden, F., Villanueva, G. L., Liuzzi, G., Thomas, I. R., et al. (2019). Water vapor vertical profiles on Mars in dust storms observed by TGO/NOMAD. *Journal of Geophysical Research: Planets*, *124*, 3482–3497. https://doi.org/10.1029/2019JE006109

Banks, P. M., & Kockarts, G. (1973). *Aeronomy*. Academic Press.

Chaffin, M. S., Deighan, J., Schneider, N. M., & Stewart, A. I. F. (2017). Elevated atmospheric escape of atmospheric hydrogen from Mars induced by high-altitude water. *Nature Geoscience*, *10*(3), 174–178. https://doi.org/10.1038/NGEO2887

Chamberlain, & Hunten (1987). *Theory of planetary atmospheres: An introduction to their physics and chemistry*. Academic Press.

Daerden, F., Neary, L., Viscardy, S., García Muñoz, A., Clancy, R. T., & Smith, M. D. (2019). Mars atmospheric chemistry simulations with the GEM-Mars general circulation model. *Icarus*, *326*, 197–224. https://doi.org/10.1016/j.icarus.2019.02.030

Encrenaz, T., Fouchet, T., Melchiorri, R., Drossart, P., Gondet, B., Langevin, Y., et al. (2006). Seasonal variations of the martian CO over Hellas as observed by OMEGA/Mars Express. *Astronomy & Astrophysics*, *459*, 265–270. https://doi.org/10.1051/0004-6361:20065586

Holmes, J. A., Lewis, S. R., Patel, M. R., & Smith, M. D. (2019). Global analysis and forecasts of carbon monoxide on Mars. *Icarus*, *328*, 232–245. https://doi.org/10.1016/j.icarus.2019.03.016

Jakosky, B. M., Slipski, M., Benna, M., Mahaffy, P., Elrod, M., Yelle, R., et al. (2017). Mar's atmospheric history derived from upper-atmosphere measurements of 38Ar/36Ar. *Science*, *355*(6332), 1408–1410. https://doi.org/10.1126/science.aai7721

Korablev, O., Montmessin, F., Trokhimovski, A., Fedorova, A., Shakun, A. V., Grigoriev, A. V., et al. (2018). The atmospheric chemistry suite (ACS) pf three spectrometers for the ExoMars 2016 trace gas orbiter. *Space Science Reviews*, *214*(1), 62. https://doi.org/10.1007/s11214-017-0437-6

Koyama, S., Terada, N., Nakagawa, H., Kuroda, T., & Sekine, Y. (2021). Stability of atmospheric redox states of early Mars inferred from time response of the regulation of H and O losses. *The Astrophysical Journal*, *912*(2), 135. https://doi.org/10.3847/1538-4357/abf0ac

Krasnopolsky, V. A. (1986). *Photochemistry of the atmospheres of Mars and Venus. Physics and Chemistry in Space* (Vol. 13). Springer. https://doi.org/10.1007/978-3-642-70401-7

Krasnopolsky, V. A. (2002). Mars' upper atmosphere and ionosphere at low, medium, and high solar activities: Implications for evolution of water. *Journal of Geophysical Research*, *107*(E12), 5128. https://doi.org/10.1029/2001JE001809

Krasnopolsky, V. A. (2006). Photochemistry of the Martian atmosphere: Seasonal, latitudinal, and diurnal variations. *Icarus*, *185*, 153–170. https://doi.org/10.1016/j.icarus.2006.06.003

Krasnopolsky, V. A. (2007). Long-term spectroscopic observations of Mars using IRTF/CSHELL: Mapping of O_2 dayglow, CO, and search for CH_4. *Icarus*, *190*, 93–102. https://doi.org/10.1016/j.icarus.2007.02.014

Krasnopolsky, V. A. (2010). Solar activity variations of thermospheric temperatures on Mars and a problem of CO in the lower atmosphere. *Icarus*, *207*, 638–647. https://doi.org/10.1016/j.icarus.2009.12.036

Lindzen, R. S. (1971). Tides and gravity waves in the upper atmosphere. In *Mesospheric models and related experiments*, (pp. 122–130). Springer. https://doi.org/10.1007/978-94-010-3114-1_8

Mahieux, A., Yelle, R. V., Yoshida, N., Robert, S., Piccialli, A., Nakagawa, H., et al. (2021). Determination of the Venus eddy diffusion profile from CO and CO_2 profiles using SOIR/Venus Express observations. *Icarus*, *361*, 114388. https://doi.org/10.1016/j.icarus.2021.114388

McElroy, M. B., & Donahue, T. M. (1972). Stability of the Martian atmosphere. *Science*, *177*(4053), 986–988. https://doi.org/10.1126/science.177.4053.986

Modak, A., López-Valverde, M., Brines, A., Stolzenbach, A., Funke, B., González-Galindo, F., et al. (2022). Retrieval of Martian atmospheric CO vertical profiles from NOMAD observations during the 1st year of TGO operations. *Journal of Geophysical Research*. Submitted for publication.

Neefs, E., Vandaele, A. C., Drummond, R., Thomas, I. R., Berkenbosch, S., & Clairquin, R. (2015). NOMAD spectrometer on the ExoMars trace gas orbiter mission: Part 1—Design, manufacturing and testing of the infrared channels. *Applied Optics*, *54*(28), 8494–8520. https://doi.org/10.1364/AO.54.008494

Olsen, K. S., Lefèvre, F., Montmessin, F., Fedorova, A. A., Trokhimovskiy, A., Baggio, L., et al. (2021). The vertical structure of CO in the Martian atmosphere from the ExoMars trace gas orbiter. *Nature Geoscience*. https://doi.org/10.1038/s41561-020-00678-w

Rodgers, C. D. (2000). Inverse methods for atmospheric sounding—Theory and practice, inverse methods for atmospheric sounding. *Series: Series on atmospheric oceanic and planetary physics*, (Vol. 2). World Scientific Publishing CO. Pte. Ltd. https://doi.org/10.1142/9789812813718

Rodrigo, R., García-Álvarez, E., López-González, J., & López-Moreno, J. J. (1990). A nonsteady one-dimensional theoretical model of Mars' neutral atmospheric composition between 30 and 200 km. *Journal of Geophysical Research*, *95*(B9), 14795–14810. https://doi.org/10.1029/90JB00158

Slipski, M., Jakosky, B. M., Benna, M., Elrod, M., Mahaffy, P., Kass, D., et al. (2018). Variability of Martian turbopause altitudes. *Journal of Geophysical Research: Planets*, *123*, 2939–2957. https://doi.org/10.1029/2018JE005704

Smith, M. D., Daerden, F., Neary, L., Khayat, A. S., Holmes, J. A., Patel, M. R., et al. (2021). The climatology of carbon monoxide on Mars as observed by NOMAD nadir-geometry observations. *Icarus*, *362*, 114404. https://doi.org/10.1016/j.icarus.2021.114404

Smith, M. D., Wolff, M. J., Clancy, R. T., & Murchie, S. L. (2009). Compact reconnaissance imaging spectrometer observations of water vapor and carbon monoxide. *Journal of Geophysical Research*, *114*, E00D03. https://doi.org/10.1029/2008JE003288

Thomas, I. R., Aoki, S., Trompet, L., Robert, S., Depiesse, C., Willame, Y., et al. (2021). Calibration of NOMAD on ESA's ExoMars trace gas orbiter: Part 1—The solar occultation channel. *Planetary and Space Science*, *105411*. https://doi.org/10.1016/j.pss.2021.105411

Thomas, I. R., Vandaele, A. C., Robert, S., Neefs, E., Drummond, R., Daerden, F., et al. (2016). Optical and radiometric models of the NOMAD instrument. Part: The infrared channels—SO and LNO. *Optics Express*, *24*(4), 3790–3805. https://doi.org/10.1364/OE.24.0037903790

Trompet, L., Vandaele, A. C., Aoki, S., Erwin, J., Thomas, I., Piccialli, A., et al. (2021). Update on CO2 and temperature profiles retrievals from NOMAD-SO on board ExoMars TGO. In *15th Europlanet Science Congress*. (EPSC2021-216). https://doi.org/10.5194/epsc2021-216

Vandaele, A. C., Korablev, O., Daerden, F., Aoki, S., Thomas, I. R., Altieri, F., et al. (2019). Martian dust storm impact on atmospheric H_2O and D/H observed by ExoMars Trace Gas Orbiter. *Nature*, *568*, 7753, 521–525. https://doi.org/10.1038/s41586-019-1097-3

Vandaele, A. C., Kruglanski, M., & De Maziere, M. (2006). *Simulation and retrieval of atmospheric spectra using ASIMUT*. Paper presented at Atmospheric Science Conference. Frascati: Eur. Space Agency.

Vandaele, A. C., Lopez-Moreno, J.-J., Patel, M. R., Bellucci, G., Daerden, F., Ristic, B., et al. (2018). NOMAD, an integrated suite of three spectrometers for the ExoMars Trace Gas Mission: Technical description, science objectives and expected performance. *Space Science Review*, *214*, 80. https://doi.org/10.1007/s11214-08-0517-2

Vandaele, A. C., Neefs, E., Drummond, R., Thomas, I. R., Daerden, F., Lopez-Moreno, J.-J., et al. (2015). Science objectives and performances of NOMAD, a spectrometer suite for the ExoMars TGO mission. *Planetary and Space Science*, *119*, 233–249. https://doi.org/10.1016/j.pss.2015.10.003

Villanueva, G. L., Liuzzi, G., Aoki, S., Brines, A., Thomas, I. R., Lopez-Valverde, M. A., et al. (2022). Isotopic ratios of water released from the northern and southern caps as measured with TGO/NOMAD. *Geophysical Research Letters*.

Yoshida, N., Nakagawa, H., Terada, N., Evans, J. S., Schneider, N. M., Jain, S. K., et al. (2020). Seasonal and latitudinal variations of dayside N_2/CO_2 ratio in the Martian thermosphere derived from MAVEN IUVS observations. *Journal of Geophysical Research: Planets*, *125*, e2020JE006378. https://doi.org/10.1029/2020JE006378

Yoshida, N., Terada, N., Nakagawa, H., Brain, D. A., Sakai, S., Nakamura, Y., et al. (2021). Seasonal and dust-related variations in the dayside thermospheric and ionospheric compositions of Mars observed by MAVEN/NGIMS. *Journal of Geophysical Research: Planets*, *126*, e2021JE006926. https://doi.org/10.1029/2021JE006926

Reference From the Supporting Information

Neary, L., & Daerden, F. (2018). The GEM-Mars general circulation model for Mars: Description and evaluation. *Icarus*, *300*, 458–476. https://doi.org/10.1016/j.icarus.2017.09.028